

RSC Advances



This is an *Accepted Manuscript*, which has been through the Royal Society of Chemistry peer review process and has been accepted for publication.

Accepted Manuscripts are published online shortly after acceptance, before technical editing, formatting and proof reading. Using this free service, authors can make their results available to the community, in citable form, before we publish the edited article. This *Accepted Manuscript* will be replaced by the edited, formatted and paginated article as soon as this is available.

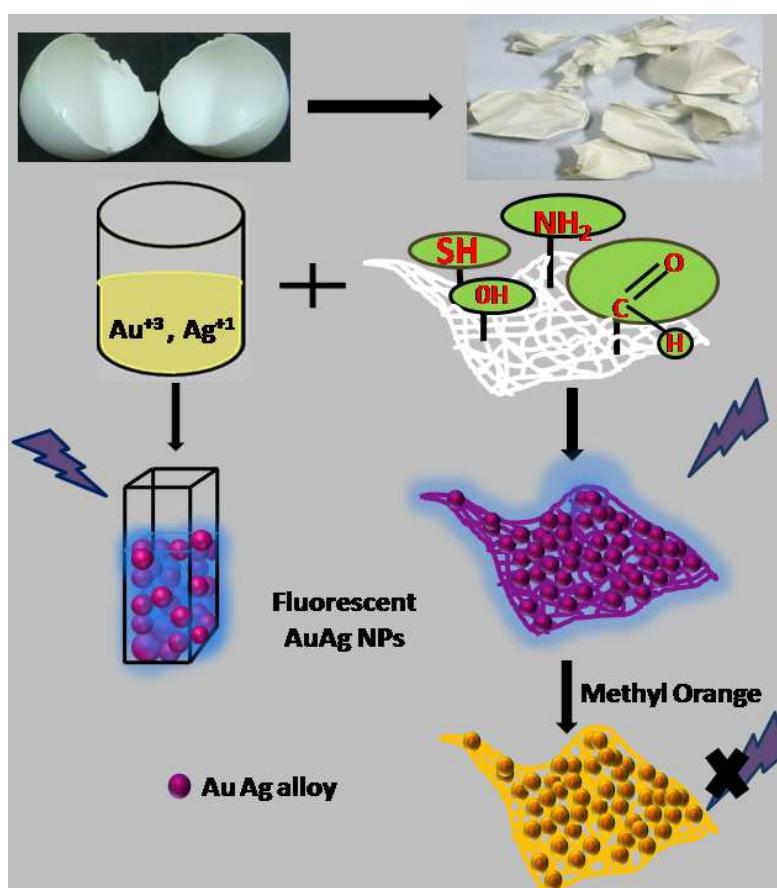
You can find more information about *Accepted Manuscripts* in the [Information for Authors](#).

Please note that technical editing may introduce minor changes to the text and/or graphics, which may alter content. The journal's standard [Terms & Conditions](#) and the [Ethical guidelines](#) still apply. In no event shall the Royal Society of Chemistry be held responsible for any errors or omissions in this *Accepted Manuscript* or any consequences arising from the use of any information it contains.

Water Soluble Blue Emitting AuAg Alloy Nanoparticles and Fluorescent Solid Platforms for Removal of Dyes from Water

Srikrishna Pramanik, Arindam Saha and Parukuttyamma Sujatha Devi *

Nano-Structured Materials Division, CSIR-Central Glass and Ceramic Research Institute,
Kolkata 700032, India.



We report here, the successful formation of blue emitting AuAg alloy nanoparticles and solid fluorescent platform by a biotemplate induced reduction process using egg shell membrane and their applications.

Water Soluble Blue Emitting AuAg Alloy Nanoparticles and Fluorescent Solid Platforms for Removal of Dyes from Water

Srikrishna Pramanik, Arindam Saha and Parukuttyamma Sujatha Devi *

Nano-Structured Materials Division, CSIR-Central Glass and Ceramic Research Institute,
Kolkata 700032, India.

Corresponding author's address:

Dr. P. Sujatha Devi, PRINCIPAL SCIENTIST, Nano-Structured Materials Division, CSIR-Central Glass & Ceramic Research Institute, 196, Raja SC Mullick Road, Jadavpur, Kolkata-700 032, India. Tel: 033-2483-8082, Fax No: +91-33-2473-0957

E-mail: psujathadevi@cgcri.res.in/psujathadevi@gmail.com

Abstract

Chicken egg shell membrane, a naturally abundant protein membrane was used to synthesize gold (Au), silver (Ag) and their bimetallic (AuAg) alloy nanoclusters at room temperature without the use of any reducing agent or catalyst. The as-formed gold and alloy clusters were highly fluorescent and exhibited intense blue emission around 435 ± 5 and 440 ± 5 nm, respectively. This is the first report confirming the formation of fluorescent alloy clusters exhibiting nanosecond life time by a biomembrane induced reduction process. We have also explored the capability of these metal clusters immobilized inexpensive ESM in removing organic dyes from water. The results confirmed that it is the strong adsorption of the dye molecules in presence of the metal particles that has helped in converting ESM to an effective platform for water purification. This process has the dual advantages of utilizing an inexpensive, abundant and eco-friendly friendly food waste- egg shell membrane- for *in-situ* reduction and formation of metal nanoparticles and utilization of the same as an effective platform for the removal of anionic dyes from waste water. Au immobilized ESM showed better efficiency in dye molecules removal compared to the Ag-ESM and AuAg-ESM membranes.

Key Words: *Egg shell membrane, protein directed synthesis, blue emission, nanosecond lifetime, pollutant dye removal*

1. Introduction

Noble metal nanoparticles and their alloy clusters are important in many areas such as medical diagnosis, controlled drug delivery, sensors and catalysis [1, 2]. Although a large number of methods are currently available for the preparation of metal/alloy nanoparticles, environment friendly techniques are poorly explored so far for this purpose. The current interest, therefore, has been focused on exploring environment friendly synthetic approaches for preparing fluorescent alloy nanoparticles/clusters for various applications. Several groups have explored protein based synthesis to produce stable fluorescent nanomaterials for applications in bio imaging [3] bio sensing [4] and metal ion detection [5]. Xie *et al.* synthesized highly fluorescent Au nanoclusters (AuNCs) exhibiting red emission using bovine serum albumin (BSA) [6], whereas Guo and Irudayaraj synthesized fluorescent Ag clusters using BSA [7] and Singh *et al.* demonstrated the synthesis of Au, Ag, AuAg alloy nanoparticles using BSA as a reducing and foaming agent [8]. Liu *et al.* reported direct synthesis of fluorescent gold nanoclusters using insulin as a template [9]. Mohanty *et al.* reported the synthesis of luminescent AuAg alloy clusters of quantum size using a protein template [10]. Gui and Jin used human serum albumin (HSA) to prepare AuAg core shell nanocrystals [11]. Recently, we have explored the use of egg shell membrane (ESM), a naturally occurring biotemplate to prepare fluorescent gold nanoparticles [12]. ESM has a 3D entangled structure of highly cross linked fibres and porous site. The super abundant, economically benign character and unique features make ESM superior than other naturally available proteins like bovine serum albumin, human serum albumin etc. The ESM is insoluble in water due to the presence of a large number of cross linked disulfide bonds [13]. The ESM is mainly consisting of glycoprotein like collagen (types I, V and X) and several other amino acids mainly glycine, cystein, uronic acid etc [14-16]. On the other hand, the presence of amino acids makes ESM a good reducing agent and stabilizer. In recent times

many research groups have used ESM to prepare AgNPs, AuNPs and other oxide materials [12, 13, 17-19]. The metal NPs immobilized ESM has shown unique advantages in biosensing [20] surface enhanced Raman spectroscopy [21] and in catalysis [22, 23]. The ESM can also act as a platform to retrieve heavy toxic metal ions such as Arsenic and Mercury from water [24]. Here, we demonstrate the simultaneous *in-situ* reduction of Au and Ag ions by the ESM resulting in the formation of highly fluorescent AuAg alloy nanoparticles and metal ions immobilized fluorescent solid ESM platforms. In addition, we also demonstrate the unique dye adsorbing capability of these metal ion immobilized ESM platforms for efficient removal of anionic dyes from waste water at room temperature. The novelty of this technique lies in the unique properties of these protein membranes since it is highly resistant to pH, safe to handle, and abundantly available in nature [13].

2. Experimental Section

2.1. Materials

AR grade chloroauric acid (HAuCl₄, S.D. Fine-Chem. Ltd, India), silver nitrate (S.D. Fine-Chem. Ltd, India), Methyl Orange (Sigma-Aldrich Chemicals) and phosphate buffer (Merck India) were used for the experiments. All reagents were used as received without further purification.

2.2 Synthesis

The cleaned egg shells were treated with dilute acetic acid (50% diluted with water) to extract the membrane (ESM) from the egg shell by soaking them for 4-6 hours. Once the calcium carbonate shell gets dissolved, the membranes were carefully collected and thoroughly washed with deionised water and then dried in air at room temperature. For the synthesis of Au and Ag nanoparticles, 0.150 gm of ESM was added to 10 ml of the individual metal ion solutions (10^{-2} M) and allowed the reaction to proceed at room temperature in dark. For the

synthesis of alloy nanoparticles, extracted dried ESM (0.150 gm) was added to a mixed solution of 5 ml of AgNO_3 and 5 ml of HAuCl_4 each of 10^{-2}M and allowed the reaction to proceed at room temperature. The concentration of the metal ions used was varied from 10^{-2}M to 10^{-3}M and exposure time for the reaction was extended up to 7 days. In the manuscript NC represents nanoclusters and NP represents nanoparticles.

2.3 Characterization

The absorption spectra were measured on SHIMADZU UV-3600 UV-Vis-NIR spectrophotometer. The solution was taken out from the impregnated membrane time to time for seven days and the absorbance was recorded at a regular interval of time. The fluorescence spectra of the same solutions were recorded at room temperature on a Steady State Spectrofluorometer (QM-40, Photon Technology International, PTI) equipped with a 150 Watt Xenon lamp as an excitation source. The emission spectra of the solution were recorded exciting at 345 nm using a fixed excitation and emission band pass of 5 nm. Raman Spectra were obtained using a Renishaw in via Reflex micro Raman spectrometer with an argon ion (785 nm) laser. The spectra were collected at a resolution of 1 cm^{-1} . The room temperature powder X-ray diffraction (XRD) was carried out on the immobilized membranes for phase identification using a Philips X-ray diffractometer (PW1730) with $\text{CuK}\alpha$ radiation at a 2θ scan rate of 2° per minute. For the Raman and XRD experiments, metal nanoparticles immobilized ESM were cut into square pieces and pasted them on thin glass plates. The transmission electron microscopy (TEM) images were taken on a TECNAI G² 30 high-resolution transmission electron microscope operating at 300 kV. For TEM study few drops of the colloidal nanoparticles were deposited on the carbon coated Cu grid and dried under an IR lamp. Field emission scanning electron micrographs (FESEM) were carried out in a Field Emission Scanning Electron Microscope (SUPRATM 35 VP; Gemini Column (Carl Zeiss

SMT)]. Time correlated single photon counting (TCSPC) measurement was performed on the water dispersions with a Horiba Jobin Yvon IBH Fluorocube apparatus after exciting the sample with 340 nm excitation lamp. The fluorescence decay was collected with a Hamamatsu MCP (R3809) photomultiplier at 435 nm, and the fluorescence decay was analyzed with IBH DAS6 software. The particle size and zeta potential of the dispersions were measured on a HORIBA (SZ-100 OZ) dynamic light scattering particle size analyser.

2.4 Dye adsorption experiment

In order to carry out the dye adsorption studies, 10 mg of metal nanoparticles immobilized ESM (Au-ESM, Ag-ESM, AuAg-ESM) were added to 10 ml of 10^{-5} M Methyl Orange (MO) solution taken in separate culture tubes covered with aluminium foil and kept them in the dark. The dye adsorption experiment was also performed in a phosphate buffer solution at a pH of 7.00 using AuAg-ESM and monitored the dye adsorption characteristics. The pH of the solution remained almost same after the addition of the membrane to the solution. The adsorption characteristics of the MO dye was monitored by recording the absorbance of the dye solution (λ_{max} at 464nm) from time to time at various time intervals. The (%) of dye removed from solution has been calculated as shown below in equation 1.

$$\text{(\% of Dye removed)} = \frac{C_0 - C_t}{C_0} \times 100 \quad (1)$$

where C_0 is the initial concentration of dye, C_t is the concentration of dye at various time intervals. Here C_0 is equivalent to A_0 the initial absorbance and C_t is equivalent to A_t the absorbance recorded at different times, where $A = \epsilon CL$, where ϵ is the molar extinction coefficient and L is the path length of the monochromatic light.

3. Results and Discussion

3.1 Optical Studies

To gain insight about the reduction process and subsequent particle formation, the *in-situ* reactions were continuously monitored by the absorbance and fluorescence spectral changes during the course of the reaction. Initial studies were carried out with gold and silver and subsequently extended the study to gold silver alloy system. The spectral changes during the interaction of ESM with different concentrations of HAuCl_4 and AgNO_3 are shown in the supporting information (Supporting Information Figs. S1 and S2, respectively). The formation of Au and Ag nanoclusters were confirmed by the characteristic Surface Plasmon Resonance (SPR) bands in the UV-Vis spectra. The spectrum recorded at room temperature as a function of time exhibited the systematic appearance of a broad band with a maximum around 535 nm for Au and 435 nm for Ag nanoclusters. The characteristic SPR peak appeared at a λ_{max} of 535 ± 2 nm for Au nanoclusters (Fig. S1) and in the case of Ag nanoclusters, the maximum absorbance was observed at 436 ± 2 nm (Fig. S2).

The spectral changes observed in a typical experiment with a 1:1 mixture of AgNO_3 solution (10^{-2} M) and HAuCl_4 (10^{-2} M) are presented in Fig. 1a. The AuAg alloy nanoclusters displayed only a single SPR peak with a maximum absorbance at around 546 ± 3 nm (Fig. 1a). This bathochromic shift compared to bare Au (535 ± 2 nm) and Ag nanoclusters (436 ± 2 nm) gives an indication of the formation of alloy clusters of larger size than the individual metal clusters. At the end of the reaction, the SPR band intensity remained invariant, attained saturation indicating the complete reduction of metal ions and formation of AuAg alloy clusters. In order to monitor the rate of reduction process, we have plotted the change in absorbance of the alloy dispersion with time as shown in Fig. S3. During the course of the experiment, the mixed metal ion solution changed colour from yellow to pink whereas the Au

and Ag solutions changed to blue and brown, respectively, as can be seen from the inset of Fig. 1b. The first observation of the colour change on the membrane confirms the formation and deposition of metal nanoclusters on the membrane. Interestingly, when the experiments were carried out at with lower concentrations of the metal ions (10^{-3} M each) there was no indication of any SPR peak formation in the absorption spectra as evident from the supporting information shown in Fig. S4. The absorption spectra of Au, Ag and the AuAg alloy dispersions shown in Fig.1b, exhibits only a single absorption band thereby confirming the formation of alloy nanoclusters.

To verify whether the alloy nanoclusters formed in solution exhibited fluorescence, we recorded the emission spectra of the colloidal solutions of Au, Ag and AuAg clusters at room temperature. The control solution of HAuCl_4 , AgNO_3 or the mixture had no visible fluorescence in the range studied (350-700 nm). Time dependent fluorescence studies during the reduction process were monitored using a 10^{-2} M metal ion solution and the results are shown in Fig. 1c. The Au nanoclusters exhibited the characteristic blue emission around 435 ± 5 nm upon excitation at 340 nm (Fig.1d). Interestingly, Ag nanoclusters did not exhibit any visible emission, whereas AuAg nanoclusters exhibited an intense blue emission at 440 ± 5 nm. In addition, the characteristic emissions of the Au nanoclusters at 540 nm and 720 nm, on excitations at 500 nm and 680 nm, respectively, were absent for the AuAg alloy clusters as clear from the supporting information Fig. S6 [12].

As evident from Fig.1 (d), the observed emission intensity varied with the concentration of the metal ions. The blue emission exhibited by gold clusters has been reported to the $\text{Au}6\text{S}$ to 6P intraband transition. Interestingly, the emission intensity was lower for the alloy nanoclusters compared to Au nanoclusters probably due to the doping of Ag into Au during the alloy formation resulting in quenching of the emission. Although the

presence of Ag in AuAg nanoclusters quenched the emission weakly, but the existence of Au in the alloy favours the excitation of d band electron to higher sp level followed by recombination of electron hole pair to give rise to the observed emission. By density functional theory, Zhang et al., have shown that Ag doping can modulate the optical properties of Au clusters [25]. Duo et al., reported aggregation between Au clusters and Ag clusters affecting the emission spectra of AuAg bimetallic nanostructures [26]. In order to further confirm that the reduction of a mixed solution of silver and gold in presence of ESM has resulted in the formation of a fluorescent alloy cluster, we have measured the fluorescence of a 1: 1 mechanical mixture of Au nanoclusters and Ag nanoclusters as shown in Fig. S7. Interestingly, the mechanical mixture did not exhibit any emission similar to the alloy clusters thereby confirming the complete quenching of the emission of Au nanoclusters in presence of Ag nanoclusters. The above result is in contrary to what we have observed for the *in-situ* formed alloy clusters, thus corroborating other results on the formation of AuAg alloy nanocluster during the *in-situ* reduction reaction. The digital images of the alloy dispersions in normal light (i) and on exposure to a UV light (ii) are presented in the inset of Fig. 1c.

During the course of the experiment, the mixed metal ion solution changed colour from yellow to colourless to deep pink as can be seen from the digital images shown in Fig. 2 and inset of Fig. 1b. The ESM surface also displayed different colours after immobilization of the metal ions. The Au-ESM turned pink, whereas the surface of ESM turned brown for Ag and bluish-red for AuAg as evident from the pictures of dried membranes shown in Fig. 2. The particle distribution representing the hydrodynamic diameter measured by the DLS technique is presented in Fig.S8a. It can be seen that the hydrodynamic diameter of the AuAg clusters (133.5nm) is much larger compared to the individual metal clusters. The alloy cluster

exhibited a broader distribution compared to the corresponding individual metal cluster dispersions. The zeta potential of the dispersions varied in the order +9.6, +3.8 and +8.2mV, respectively, for Au, Ag and AuAg clusters, confirming their positively charged surface characteristics (Fig.S8b).

Interestingly, when we have carried out the emission experiments with lower concentrations of the metal ions (10^{-3} M each), both Au nanocluster and alloy nanocluster exhibited strong visible emission as evident in curves 3 & 4 of Fig.1d. It is worth noting the absence of a strong SPR band at lower concentrations (Fig.S4). In order to understand the effect of particle size on the optical properties, we have separated the larger and smaller particles by centrifuging the as-formed dispersion (10^{-2} M) at 10000 rpm for 20 minutes. The supernatant and the precipitates were separately characterized via absorption and emission measurements. It has been found that the supernatant mostly composed of smaller nanoclusters of average size around 36.7 nm after 3 days and 47.2 nm after 7 days as evident from the DLS data shown in Fig. S9 a&d. The precipitate, on the other hand, exhibited larger sized clusters of 84 nm after 3 days and 104 nm after 7 days as shown in Fig. S9 a&d. In Fig. S9 b&e, the UV-Vis spectra of the smaller and larger clusters collected at 3rd and 7th days are presented. Similarly, in Fig. S9 c&f, the emission data of the smaller and larger clusters are presented. Compared to the as-formed clusters, the separated fractions exhibited slightly different absorbance maxima of 545 ± 2 nm for larger sized fraction and 530 ± 2 nm for the smaller sized fraction. There was not much difference in the absorbance maximum with time except a reduction in the absorbance. Interestingly, the emission maxima of all the samples remained the same. It is evident that the smaller particles exhibited stronger emission compared to the larger particles (Fig.S9 c &f), without any shift in the peak position. The larger nanoparticles are expected to quench the fluorescence of smaller particles, and

accordingly, we have noticed a reduction in the fluorescence intensity after 7 days of the reaction. It is very hard to control the invariant growth of the particles as ESM contains several amino acids with binding or reducing sites with different reducing capability resulting in particles of variable size and shape forming various metallic clusters.

Time correlated single photon counting (TCSPC) measurement was performed by exciting the sample with 340 nm excitation lamp. The fluorescence decay was collected at 435 nm (Fig. 3). Au nanoclusters exhibited third order exponential decay with $\tau_1 = 2.572$ ns, $\tau_2 = 9.9$ ns and $\tau_3 = 0.3$ ns and their relative percentages were 43.82, 38.94 and 17.24, respectively. From this data, it is clear that major contribution in the average lifetime was from τ_1 and τ_2 which was around 84% of the total lifetime and both of them were in nanosecond order. The AuAg alloy also exhibited third order exponential decay with $\tau_1 = 1.6$ ns, $\tau_2 = 7.1$ ns and $\tau_3 = 0.125$ ns and their relative percentages were 37.68, 22.85 and 39.47, respectively. In this case, the major contributions were from τ_1 and τ_3 which was around 76% of the total lifetime and an order less than that of Au nanoparticles. The reduced lifetime in alloy nanoclusters is caused by the incorporation of Ag in Au nanoparticles which induce quenching of fluorescence from Au nanoparticles, resulting in shorter lifetimes. These findings further prove the successful synthesis of AuAg alloy nanoclusters by ESM.

3.2. Morphological Evaluation

The exact particle size and morphology of the synthesized nanoparticles were monitored using Transmission Electron Microscopy (TEM). In Fig. 4a-c, typical bright field images of Au, Ag and AuAg alloy nanoclusters are presented. A typical image of the Au colloidal solution (Fig. 4a) showed the presence of a large number of spherical and triangular particles of size smaller than 50 nm. The silver particles of size within 5-20 nm on the other hand grew and assembled into islands of flowers as shown in Fig. 4b. Most of the alloy particles are

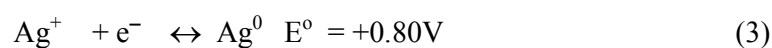
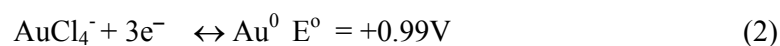
spherical or elongated in shape (Fig.4c). In Fig. 4 d-f, the particle size distribution generated from the TEM images using image j software is presented. the distribution of particles are within 5-50 nm for Au, 3-30 nm for Ag and 5-100 nm for AuAg, respectively. The average size distribution from the TEM images (Fig. 4d-f) shows average sizes of 18.12 nm, 12.4 nm and 42.21 nm, respectively, for Au, Ag and AuAg nanoclusters. The alloy clusters are much larger in size compared to the corresponding individual metal clusters. The AuAg dispersion exhibited the presence of both larger and finer particles. The high resolution transmission electron microscopic (HRTEM) images and selected area electron diffraction (SAED) patterns of AuAg nanoparticles are shown in Fig. 4g and h, respectively. Energy dispersive X-ray analysis (EDAX) was performed on the selected particles to further confirm the presence of both Au and Ag in the alloy nanoparticles (Fig. S10). The characteristic peaks of Au at 2.195 KeV, 9.72 KeV and Ag at 2.98 KeV, 3.2 KeV confirmed the presence of both gold and silver in the alloy particles [27, 28]. The crystalline nature of the AuAg alloy is confirmed through HRTEM image shown in Fig. 4g. The measured spacing between adjacent lattice fringes of 0.235nm is compatible to the 111 reflection of Au (Fig.S11) and Ag (Fig. S12) of face centred cubic structure. Au and Ag have a similar ionic radii of 1.44 Å, and hence the lattice fringes does not show much difference compared to the corresponding metal nanoparticles. The SAED pattern of AuAg alloy in Fig. 4h also confirms the successful formation of the crystalline alloy nanoparticles. The TEM image of the alloy in Fig.4c, clearly confirms the formation of clusters. In Fig.4i, an expanded TEM picture of a single particle is shown which clearly indicates the formation of twinned nanostructures. The FCC metals like Au and Ag are known to form twinned structures. In here, due to the slow reduction of the metal ions by ESM results in slow nucleation and restricts the separate nucleation of Ag or Au and formed twinned AuAg alloy particles.

Micro structural change and morphology of the *in-situ* generated particles embedded on the Au-ESM, Ag-ESM and AuAg-ESM were characterized by FESEM at different magnifications. From the SEM images it can be clearly seen that ESM has an interlinked net like fibre structure. In Fig. 5a and b the spherical nature of the finely deposited particles on the fibrous network of membrane surface can be clearly seen. The EDAX spectrum recorded on the membrane confirms the presence of both Au and Ag on the solid membrane (Fig. S13). The X-ray powder diffraction (XRD) analysis further proved the crystalline nature of the metal particles immobilized on the surface of ESM. The natural ESM was amorphous to X-rays whereas the metal nanoparticle immobilized membranes were highly crystalline in nature as evident from the XRD patterns shown in Fig. 5c. The AuAg-ESM exhibited characteristic diffraction peaks corresponding to the 111 and 200 planes at 2θ values of 38.37° and 44.46° , respectively, of metallic particles. From Fig. 5c, it can be seen that the diffraction peaks are slightly shifted in the case of AuAg-ESM compared to Au-ESM and Ag-ESM. The 2θ value of (111) plane appeared at 38.18° and 38.26° , respectively, for Au (JCPDS 04-0784) and Ag (JCPDS 02-1098) and the (200) plane appeared at 44.39° for Au and at 44.51° for Ag, respectively. From these results, it can be confirmed that the nanoparticles deposited on the ESM contain both Ag and Au.

3.3. Raman Studies

Raman spectroscopy is highly useful to characterize disulfides and thiols present in ESM, because the Raman bands are more intense compared to their infrared absorption bands. Since ESM contains Keratin having disulphide bonds, we used Raman spectroscopy to characterize the ESM and metal immobilized ESM. In Fig. 5d the Raman spectrum of the bare ESM and metal nanoparticle incorporated ESM is presented. Several peaks were observed in normal ESM, which were tentatively assigned to the presence of various S-S, C-S and amide linkages [29]. The weak bands at 510 and 540 cm^{-1} corresponds to the presence of

S-S stretching bonds confirming the presence of disulphide bonds, band at 756 cm^{-1} corresponding to C-S bonds, 1450 cm^{-1} corresponding to C-H bonds, and many smaller and weaker stretching bands at 1247 , 1335 , 1460 , 154 and 1660 cm^{-1} corresponding to various amide linkages present in the ESM [28]. It is highly interesting to notice the dramatic change in the Raman intensity of the ESM resulting in a broad band in the $1000\text{-}1700\text{ cm}^{-1}$ on deposition of the metal nanoparticles. This clearly confirms that after the reduction of metal ions the characteristic features of the ESM disappears. The new broad peak appeared at 1360 cm^{-1} , 1316 cm^{-1} and 1322 cm^{-1} , respectively, for the Au-ESM, Ag-ESM and AuAg-ESM. The intensity was highest for AuAg-ESM upon 785 nm laser excitation for 10 sec . The change in the intensity of these bonds could possibly associate with changes in the functional groups of proteins present on the ESM as a result of the deposition of metal ions. This could also give an indication of the reaction of various functional groups with the metal nanoparticles. The work is in progress to explore the application of these metal coated membranes for SERS applications. The ESM structure mainly contains glycoproteins like collagen and several amino acids like glycine, cystein, uronic acid etc. During the reaction, metal ions (Au^{+3} , Ag^{+1}) are readily adsorbed on the porous ESM surface. The functional groups present on the proteins such as $-\text{NH}_2$, $-\text{SH}$, $-\text{CHO}$, $-\text{OH}$ groups reduced the metal ions to form metal nanoparticles or alloy nanoparticles. It is interesting to note that the ESM proteins are insoluble in water and this rule out the influence of such protein molecules exhibiting fluorescence in the present case. Though, each metal ion bears a different standard reduction potential as shown below, the ESM is still capable of reducing individual metal ions simultaneously, resulting in the formation of alloy particles as has been demonstrated here.



Since the reduction potential of Au^+/Au is higher than that of Ag^+/Ag , Au nucleation could start in the initial phase. The *in-situ* formed Au nuclei could further induce the reduction of Ag^+ through electron transfer finally resulting in simultaneous nucleation of both Au and Ag and the formation of AuAg alloy nanoparticles and clusters.

The main constituents of ESM are glycine, alanine and uronic acid in addition to the presence of several bacteriolytic enzymes such as lysozyme and glucosaminidase. Such a structure with a number of amino, carboxyl and carbonyl functional groups on the ESM fibres could get charged under the acidic conditions of our experiments and could bring the metal ions closer to the surface via hydrophobic interaction or hydrogen bonding resulting in surface adsorption. Once adsorbed on the membrane, the aldehyde ($-\text{CHO}$) and amino ($-\text{NH}_2$) functional groups may act as reducing agents to reduce the adsorbed ions to metal nanoparticles. Our experimental observations clearly confirmed that the *in-situ* reduction in presence of ESM could in fact produce fluorescent Au and AuAg nanoparticles in solution without the use of any capping/ reducing agent for inducing the formation of fluorescent metal clusters. To the best of our knowledge, this is the first report confirming the formation of fluorescent AuAg alloy nanoparticles exhibiting nanosecond life time by a biotemplate, such as ESM, induced reduction process. However, the reduction process is slow due to the weak reducing power of the functional groups present in the membrane and thus it takes longer time to complete the reduction reaction as shown in Fig.S4.

3.4. Application of the metal atoms immobilized ESM as a Sorbent for Removal of Dyes

In order to explore the practical application of the green synthesized metal immobilized ESM, we studied the pollutant dye adsorption capability of the membranes. To monitor the dye removal capability of Au, Ag and AuAg–ESM immobilized membranes, 10 mg of the nanoparticle immobilized ESM was treated with 10 ml of 10^{-5}M sodium 4-[(4-

dimethylamino) phenylazo]benzene sulfonate commonly known as Methyl Orange (MO) dye solution in the dark. We have chosen the anionic dye, MO, with the anticipation of the interaction of the dye molecules with the functional groups present on the surface of ESM and on the charged nanoparticles. The reaction was monitored by measuring the change in the absorbance maxima (λ_{max}) of the dye around 464 nm. Soon after the addition of the membrane to the dye solution, a bathochromic shift in the λ_{max} was observed as evident from Fig.6a-c. The bathochromic shift was highest in presence of Au-ESM where the absorption maxima shifted 20 nm towards the higher wavelength. No further shift in the peak position was noticed with time, except the initial peak shift. However, as evident from the absorption spectra, a systematic decrease in the intensity was noticed indicating the adsorption of dye molecules on the membrane. Interestingly, the Au-ESM exhibited the highest adsorption capacity among the investigated membranes. The observed bathochromic shift is mainly attributed to the change in the pH of the solution. The pH of the initial MO solution in double distilled water was 6.9 which changed to 3.4, 3.89 and 3.56 soon after the addition (5 minutes) of Au-ESM, Ag-ESM and AuAg-ESM, respectively. Along with change in pH, the colour of the MO solution changed from yellow for the initial solution to orange after the addition of the membrane (inset of Fig.6 a-c, 1). Finally, the adsorption gets saturated after 24 hours resulting in complete discolouration of the dye solution. The digital image (2) is the reaction media after 24 hours exhibiting a colourless solution is indicative of complete adsorption of the dye molecules on the membrane. The sequential decrease in the concentration of dye is clearly observed from the C_t/C_0 vs. time (Fig. 6d) plot. From Fig. 6e, it can be observed that the (%) dye removal capability of Au-ESM is maximum (90.43%) followed by Ag-ESM (82%), and AuAg-ESM (80.26%). In order to confirm the enhanced dye adsorption property of the Au, Ag and AuAg nanoparticles immobilized ESM, we also performed the same experiments with bare ESM. Interestingly, even after 24 hours of

immobilization also, only 10.53 % of the MO dye got adsorbed (Fig.6f) on the bare ESM compared to 90% dye adsorption on Au-ESM. Though ESM has been reported to act as an adsorbent material for direct red and acid blue dyes [30], for anionic dyes like MO, it exhibited very poor adsorption characteristics. We also carried out the experiments in a phosphate buffer solution of pH~ 7. In the buffer solution also, the metal nanoparticle immobilized ESM exhibited good adsorption property which is evident from the reduction in the absorbance of MO at 464 nm (Fig. S14). However, the adsorption was higher in distilled water compared to the buffer solution.

We also treated the metal nanoparticles immobilized ESM with a cationic dye (Methyl Violet) under similar experimental conditions. Interestingly, no dye adsorption was observed with MV dye molecules as evident from the absorbance data shown in the supporting information (Fig. S15). Interaction of the particle dispersion with dye was also extremely poor with no change in the dye absorbance, except a minor shift in the λ_{\max} position (Fig. S16). Though the metal nanoparticles were reported to be active in enhancing the degradation of MO (31), in our case we anticipated an enhanced adsorption of the dye molecules on the ESM in presence of the metal nanoparticles. In order to prove that it is not a catalytic degradation, we have carried out desorption studies with the MO adsorbed membranes. After completion of the dye adsorption, metal nanoclusters immobilized ESM were taken out and dried at RT. The dried membranes were added to 0.005 M NaOH solution to study the dye desorption experiments. During this process colour of the solution changed from colourless to yellow and the characteristic absorbance peak intensity of MO in solution gradually increased. This is due to the desorption of the anionic dye molecules adsorbed on the nanoclusters immobilized ESM releasing to the solution. The desorption was completed within 2 hours. The data for the desorption experiments are presented in Fig.

S17. In Fig.7, the percentage adsorption and desorption are compared in a bar diagram. Almost 88.2% of the adsorbed dye molecule got desorbed from Au-ESM where as from AuAg-ESM and Ag-ESM the desorption rate was only 74% and 68.38%, respectively. A minimum amount of the dye still remain adsorbed on the ESM substrates probably due to their stronger interaction with the metal nanoparticles. A schematic of the interaction between metal nanoparticles immobilized ESM and MO dye is presented in Fig.8. Our experiments with this naturally occurring biomembrane confirmed that metal ion incorporated ESM could be a cost effective, eco-friendly and safe material to remove pollutant dyes from waste water.

4. Conclusions

The ESM mediated route has led to the formation of AuAg nanoclusters with distinct fluorescence that could have tremendous impact on biomedical applications. To the best of our knowledge, this is the first report on the formation of fluorescent alloy nanoparticles by *in-situ* reduction of metal ions using a naturally and abundantly available biotemplate without the use of any catalyst, or chemical reducing agent at ambient conditions. We have also explored the capability of these metal particles immobilized inexpensive ESM in removing organic anionic dyes from water. The ESM without the nanoparticles were not effective in dye adsorption. These results confirmed that it is the enhanced adsorption of the dye molecules in presence of the metal particles that has helped in converting ESM an effective platform for water purification. This process has a dual advantage of utilizing the inexpensive and abundant food waste ESM for immobilizing the metal nanoparticles and at the same time using the same as an effective platform for the removal of organic dyes from water.

Acknowledgements

PSD acknowledges the financial support from Council of Scientific and Industrial Research (CSIR) through the network project MULTIFUN CSC 0101. SP acknowledges CSIR Govt. of India for the award of Junior Research Fellowship (JRF) through the National Eligibility Test, AS acknowledges CSIR Govt. of India for Nehru Post-Doctoral fellowship.

Supplementary Data

In-situ formation of metal nanoclusters by UV-Vis data, emission data of fluorescent AuNCS, and alloy NCs, DLS and zeta potential data, EDAX and HRTEM data on the synthesized nanoparticles, UV-Vis data depicting the interaction of membranes with MO dye in buffer solution, MV dye in distilled water and interaction of AuAg nanoclusters with MO dye, and desorption experiments.

References

- 1 C. N. R. Rao, G. U. Kulkarni, P. J. Thomas and P. E. Edwards, *Chem. Soc. Rev.*, 2000, **29**, 27-35.
- 2 M. C. Daniel and D. Astruc, *Chem. Rev.*, 2004, **104**, 293-346.
- 3 Z. Luo, K. Zheng, J. Xie, *Chem. Commun.* 2014, **50**, 5143-5155.
- 4 S. Zeng, D. Baillargeat, H.P. Ho, K.T. Yong, *Chem. Soc. Rev.*, 2014, **43**, 3426-3442.
- 5 X. Yang, L. Yang, Y. Dou, S. Zhu, *J. Mater. Chem. C.*, 2013, **1**, 6748-6751.
- 6 J. Xie, Y. Zheng, J. Y. Ying, *J. Am. Chem. Soc.*, 2009, **131**, 888-889.
- 7 C. Guo, J. Irudayaraj, *Anal. Chem.*, 2011, **83**, 2883-2889.
- 8 A. V. Singh, B. M. Bandgar, M. Kasture, B. L. V. Prasad, M. Sastry, *J. Mater. Chem.*, 2005, **15**, 5115-5121.
- 9 C.L. Liu, H.T. Wu, Y.H. Hsiao, C.W. Lai, C.W. Shih, Y.K. Peng, K.C. Tang, H.W. Chang, Y.C. Chien, J.K. Hsiao, J.T. Cheng, P.T. Chou, *Angew. Chem., Int. Ed.*, 2011, **50**, 7056-7060.

- 10 J.S. Mohanty , P.L. Xavier , K. Chaudhari, M.S. Bootharaju, N. Goswami, S.K. Pal , T. Pradeep, *Nanoscale*, 2012, **4**, 4255-4262.
- 11 R. Gui, H. Jin, *Analyst*, 2013, **138**, 7197-7205.
- 12 P. S. Devi, S. Banerjee, S. R. Chowdhury, G. S. Kumar, *RSC Adv.*, 2012, **2**, 11578-11585.
- 13 M. Balaz, *Acta Biomaterialia*, 2014, **10**, 3827-3843.
- 14 M. Wong, M. J. C. Hendrix, K. von der Mark, C. Little, R. Stern, *Dev. Biol.*, 1984, **104** , 28-36.
- 15 J. L. Arias, M. S. Fernandez, J. E. Dennis, A. I. Caplan, *Connect. Tissue Res.*, 1991, **26**, 37-45.
- 16 N. Li, L.N. Niu, Y.P. Qi, C.K.Y. Yiu, H. Ryou, D. D. Arola, J.H. Chen, D.H. Pashley, F. R. Tay, *Biomaterials*, 2011, **32**, 8743-8752.
- 17 C. Shao, B. Yuan, H. Wang, Q. Zhou, Y. Li, Y. Guan, Z. Deng, *J. Mater. Chem.*, 2011, **21**, 2863-2866.
- 18 M. Liang, R. Su, R. Huang, W. Qi, Y. Yu, L. Wang, Z. He, *ACS Appl. Mater. Interfaces*, 2014, **6**, 4638-4649.
- 19 Q. Dong, H. Su, D. Zhang, Z. Liu, Y. Lai, *Microporous and Mesoporous Materials.*, 2007, **98**, 344-351.
- 20 B. Zheng, L. Qian, H. Yuan, D. Xiao, X. Yang, M. C. Paau, M. M. F. *Talanta*, 2010, **82**, 177-183.
- 21 P.Y. Lin, C.W. Hsieh, P. C. Tsai, S. Hsieh, *Chem.phys.chem.*, 2014, **15**, 1577-1580.
- 22 R.M. Rezaei, H.Razmi, S.D. Reyhan, *Colloids and Surface B: Biointerfaces*, 2014, **118**, 188-193.
- 23 R. Mallampati, S. Valiyaveetil, *ACS Sustainable Chem. Eng.*, 2014, **2**, 855-859.

- 24 R. Shoji, T. Miyazaki, T. Niinou, M. Kato, H. Ishii, *J. Mater. Cycles Waste Manage.* 2004, **6**, 142-146.
- 25 X. Zhang, M. Guo, D. W, P. Liu, Y. Sun, L.Zhang, Y. She, Q. Liu, F. Fan, *Int. J. Mol. Sci.* 2011, **12**, 2972-2981.
- 26 X. Dou, X. Yuan, Y. Yu, Z. Luo, Q. Yao, D. T. Leong , J. Xie., *Nanoscale*, 2014, **6**, 157-161.
- 27 A. Kumar, P. K. Vemula, P. M. Ajayan, G. John, *Nat. Mater.*, 2008, **7**, 236-241.
- 28 S. K. Das, A. R. Das, A. K. Guha, *Langmuir*, 2009, **25**, 8192-8199.
- 29 S. J. Hamdrakas, E. L. Kamitsos, A. Papaikolaou, *Int. J. Biol. Macromol.*, 1984, **6**, 333-336.
- 30 M. Arami, N. Y. Limaee, N.M. Mahmoodi , *Chemosphere*, 2006, **65**, 1999–2008.
- 31 N. Gupta, H.P. Singh, R.K. Sharma, *J. Mol. Catal. A: Chemical*, 2011, **335**, 248-252.

Figure Captions

Figure 1: (a) UV-Vis absorption spectra of the Au-Ag mixture in presence of ESM (b) Comparison of UV-Vis spectra of the Au NPs, AuAg Nps and Ag Nps after the end of the reaction. The inset shows the image of colloidal (1)Au, (2)AuAg, (3)Ag NPs. (c) fluorescence spectra of AuAg alloy solution (10^{-2} M HAuCl₄+ 10^{-2} M AgNO₃ +ESM) at 345 nm excitation. Curves (1-6) represent the emission peak for 1-7 days and (d)The fluorescence spectra of Au, Ag and their bimetallic alloy solution of various concentrations. The inset in (c) shows the digital image of the dispersions in normal light and on exposure to UV light (blue colour).

Figure 2: A schematic of the formation of metal nanoclusters and metal immobilized ESM.

Figure 3: Comparison of photoluminescence lifetime decay of Au and AuAg alloy nanoparticles. Alloy nanoparticles show shorter lifetime compared to Au nanoparticles.

Figure 4: TEM images of (a) Au (b) Ag (c)AuAg alloy NPs; Particle size distribution of (d)Au, (e) Ag and (f) AuAg alloy (g) and (h) represent the HRTEM image and SAED pattern of AuAg alloy and (i) TEM image of a single particle of AuAg alloy.

Figure 5: (a), (b) FESEM images of Au-Ag-ESM. (c) XRD patterns for Au-ESM, Ag-ESM and AuAg-ESM. (d) Raman spectra of normal ESM and Au, Ag, Au-Ag alloy immobilized membrane. The inset image shows the blue emitting AuAg-ESM membrane under UV light.

Figure 6: (a), (b), (c) represents the absorption spectra of the MO dye solution in presence of Au-ESM, Ag-ESM, AuAg-ESM, respectively, inset shows images of the MO dye solution just after 5 minutes (1) and the dye solution after 24 hrs (2), (d) Ct/C₀ values of MO in presence of the membrane, (e) % of dye removed from each of the Au, Ag and AuAg ESM, inset in Fig. 6e, 1 and 2 are the images of the AuAg-ESM membrane in presence of UV light before and after dye adsorption and f) Absorption spectra of the MO in presence of bare ESM confirming poor adsorption.

Figure 7:Percentage of the dye adsorbed and desorbed by the AuESM, AuAgESM and AgESM membranes.

Figure 8: Schematic of the interaction of metal nanocluster-ESM and the MO dye molecule.

Figure Captions

Figure 1: (a) UV-Vis absorption spectra of the Au-Ag mixture in presence of ESM (b) Comparison of UV-Vis spectra of the Au NPs, AuAg Nps and Ag Nps after the end of the reaction. The inset shows the image of colloidal (1)Au, (2)AuAg, (3)Ag NPs. (c) fluorescence spectra of AuAg alloy solution (10^{-2} M $\text{HAuCl}_4 + 10^{-2}$ M AgNO_3 +ESM) at 345 nm excitation. Curves (1-6) represent the emission peak for 1-7 days and (d)The fluorescence spectra of Au, Ag and their bimetallic alloy solution of various concentrations. The inset in (c) shows the digital image of the dispersions in normal light and on exposure to UV light (blue colour).

Figure 2: A schematic of the formation of metal nanoclusters and metal immobilized ESM.

Figure 3: Comparison of photoluminescence lifetime decay of Au and AuAg alloy nanoparticles. Alloy nanoparticles show shorter lifetime compared to Au nanoparticles.

Figure 4: TEM images of (a) Au (b) Ag (c)AuAg alloy NPs; Particle size distribution of (d)Au, (e) Ag and (f) AuAg alloy (g) and (h) represent the HRTEM image and SAED pattern of AuAg alloy and (i) TEM image of a single particle of AuAg alloy.

Figure 5: (a), (b) FESEM images of Au-Ag-ESM. (c) XRD patterns for Au-ESM, Ag-ESM and AuAg-ESM. (d) Raman spectra of normal ESM and Au, Ag, Au-Ag alloy immobilized membrane. The inset image shows the blue emitting AuAg-ESM membrane under UV light.

Figure 6: (a), (b), (c) represents the absorption spectra of the MO dye solution in presence of Au-ESM, Ag-ESM, AuAg-ESM, respectively, inset shows images of the MO dye solution just after 5 minutes (1) and the dye solution after 24 hrs (2), (d) C_t/C_0 values of MO in presence of the membrane, (e) % of dye removed from each of the Au, Ag and AuAg ESM, inset in Fig. 6e, 1 and 2 are the images of the AuAg-ESM membrane in presence of UV light before and after dye adsorption and f) Absorption spectra of the MO in presence of bare ESM confirming poor adsorption.

Figure 7:Percentage of the dye adsorbed and desorbed by the AuESM, AuAgESM and AgESM membranes.

Figure 8: Schematic of the interaction of metal nanocluster-ESM and the MO dye molecule.

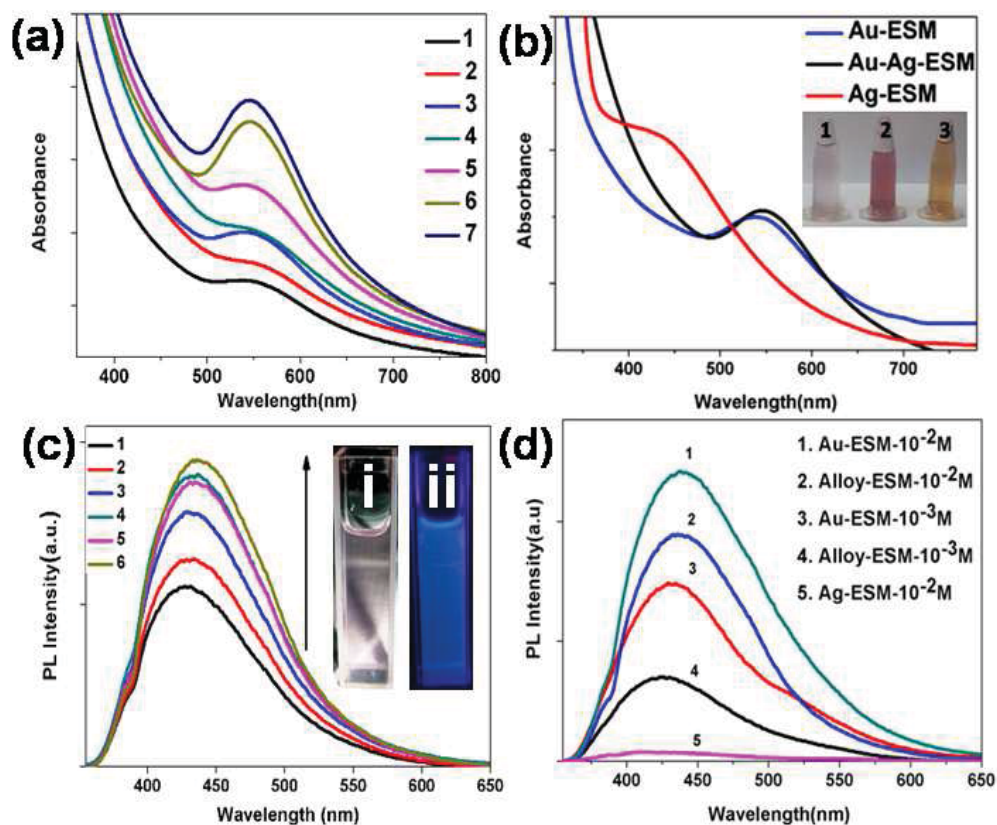


Figure 1: (a) UV-Vis absorption spectra of the Au-Ag mixture in presence of ESM (b) Comparison of UV-Vis spectra of the Au NPs, AuAg Nps and Ag Nps after the end of the reaction. The inset shows the image of colloidal (1)Au, (2)AuAg, (3)Ag NPs. (c) fluorescence spectra of AuAg alloy solution (10^{-2} M $\text{HAuCl}_4 + 10^{-2}$ M $\text{AgNO}_3 + \text{ESM}$) at 345 nm excitation. Curves (1-6) represent the emission peak for 1-7 days and (d) The fluorescence spectra of Au, Ag and their bimetallic alloy solution of various concentrations. The inset in (c) shows the digital image of the dispersions in normal light and on exposure to UV light (blue colour).

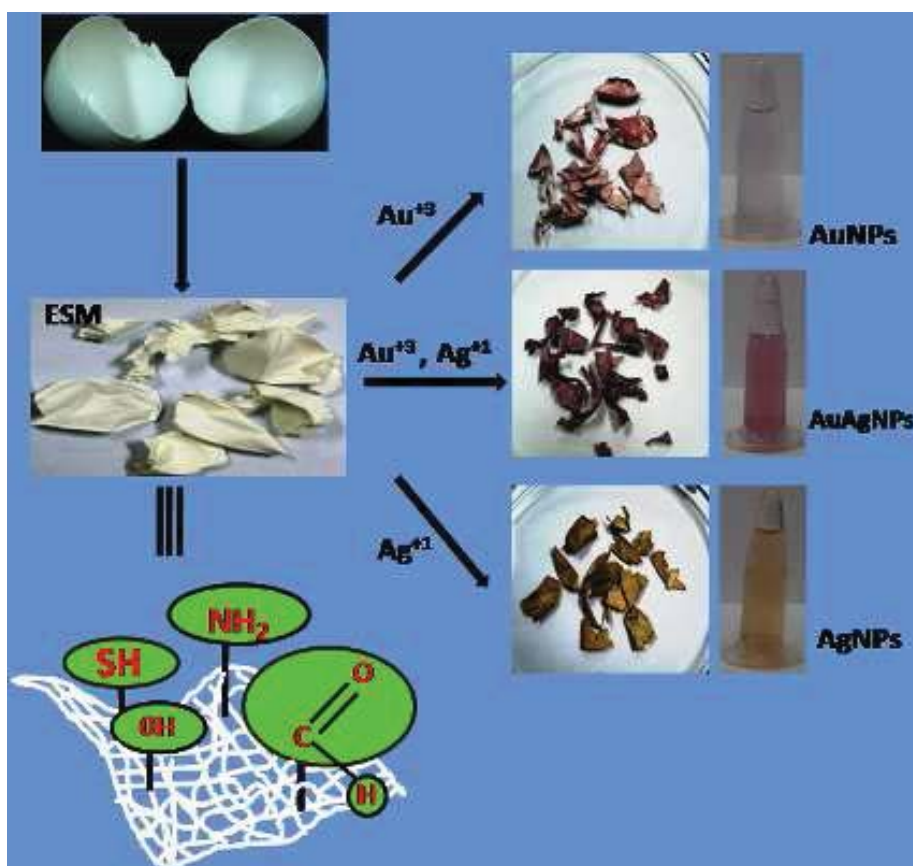


Figure 2: A schematic of the formation of metal nanoclusters and metal immobilized ESM.

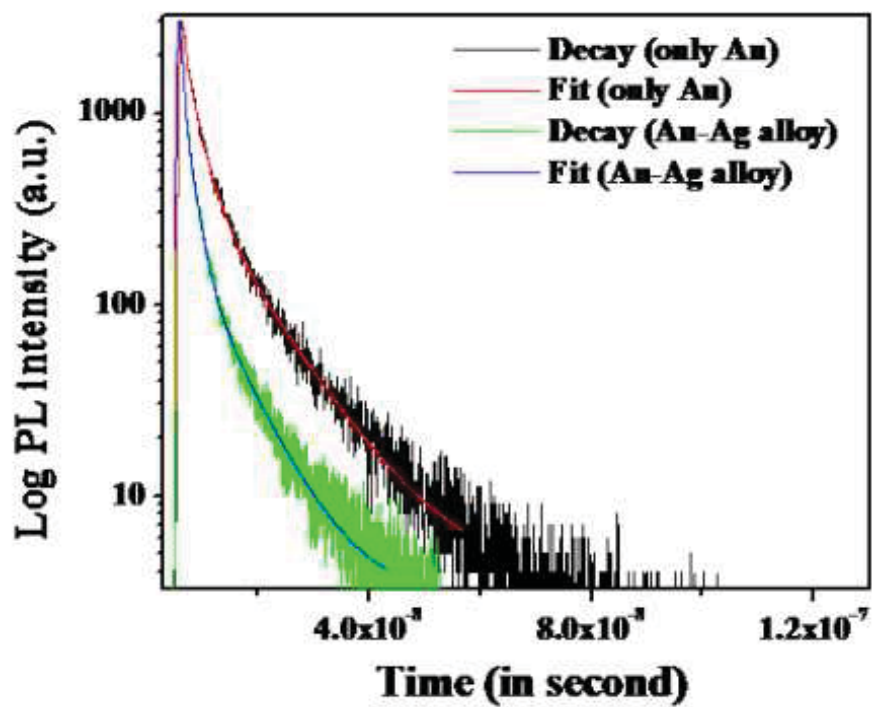


Figure 3: Comparison of photoluminescence lifetime decay of Au and AuAg alloy nanoclusters. Alloy show shorter lifetime compared to only Au nanoclusters.

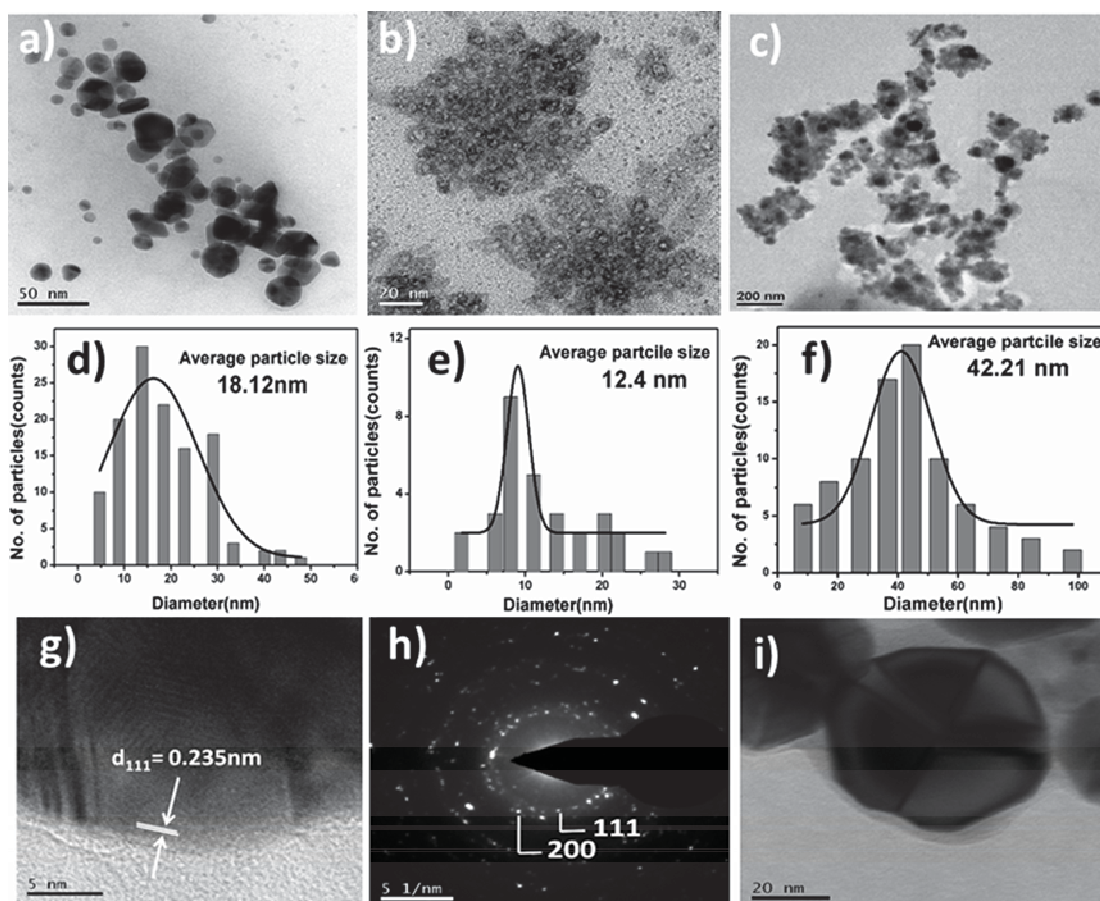


Figure 4: TEM images of (a) Au (b) Ag (c) AuAg alloy NPs; Particle size distribution of (d) Au, (e) Ag and (f) AuAg alloy (g) and (h) represent the HRTEM image and SAED pattern of AuAg alloy and (i) TEM image of a single particle of AuAg alloy.

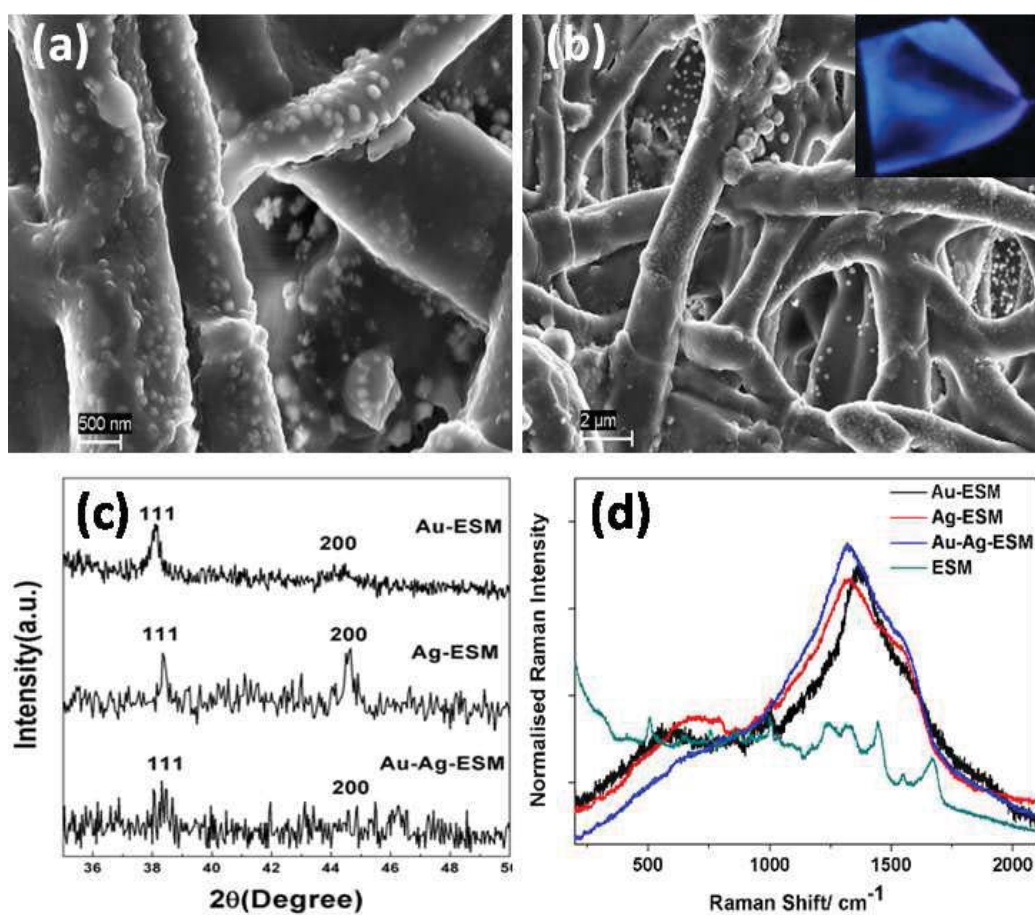


Figure 5: (a), (b) FESEM images of Au-Ag-ESM. (c) XRD patterns for Au-ESM, Ag-ESM and AuAg-ESM. (d) Raman spectra of normal ESM and Au, Ag, Au-Ag alloy immobilized membrane. The inset image shows the blue emitting AuAg-ESM membrane under UV light.

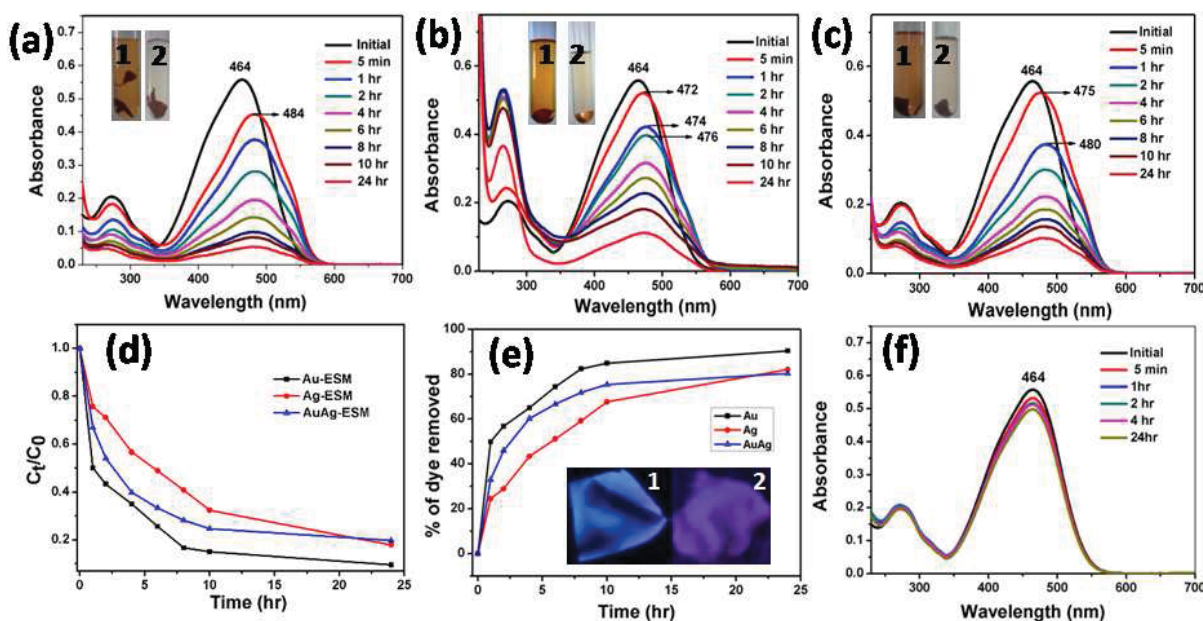


Figure 6: (a), (b), (c) represents the absorption spectra of the MO dye solution in presence of Au-ESM, Ag-ESM, AuAg-ESM, respectively, inset shows images of the MO dye solution just after 5 minutes (1) and the dye solution after 24 hrs (2), (d) C_t/C_0 values of MO in presence of the membrane, (e) % of dye removed from each of the Au, Ag and AuAg ESM, inset in Fig. 6e, 1 and 2 are the images of the AuAg-ESM membrane in presence of UV light before and after dye adsorption and f) Absorption spectra of the MO in presence of bare ESM confirming poor adsorption.

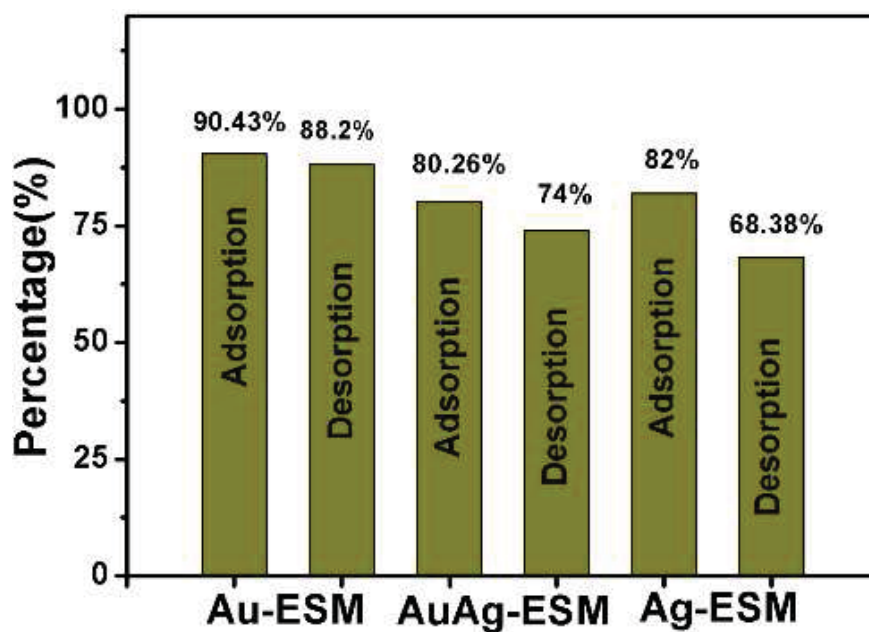


Figure 7:Percentage of dye adsorbed and desorped by Au-ESM, AuAg-ESM and Ag-ESM membranes.

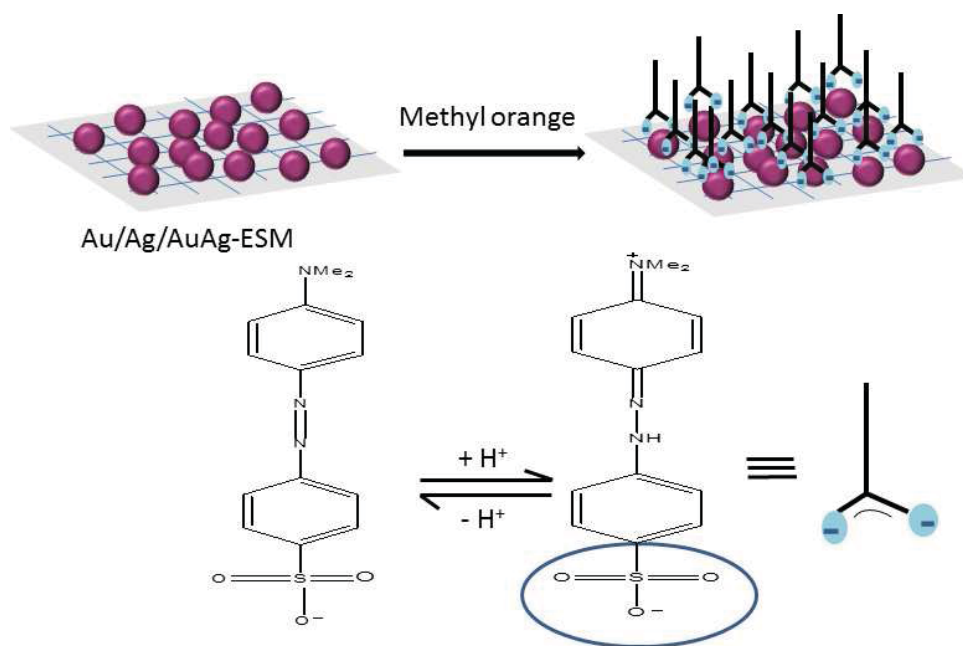


Figure 8. Schematic of the interaction of metal nanocluster-ESM and the MO dye molecule.